

Anomalous reflection and vortex beam generation by multi-bit coding acoustic metasurfaces

Cite as: Appl. Phys. Lett. **114**, 091905 (2019); <https://doi.org/10.1063/1.5087636>

Submitted: 03 January 2019 . Accepted: 24 February 2019 . Published Online: 08 March 2019

Ya Zhang , Boyang Xie , Wenwei Liu, Hua Cheng, Shuqi Chen , and Jianguo Tian



View Online



Export Citation



CrossMark

Applied Physics Reviews
Now accepting original research

2017 Journal
Impact Factor:
12.894

AIP
Publishing

Anomalous reflection and vortex beam generation by multi-bit coding acoustic metasurfaces

Cite as: Appl. Phys. Lett. **114**, 091905 (2019); doi: [10.1063/1.5087636](https://doi.org/10.1063/1.5087636)

Submitted: 3 January 2019 · Accepted: 24 February 2019 ·

Published Online: 8 March 2019






View Online



Export Citation



CrossMark

Ya Zhang,¹  Boyang Xie,¹  Wenwei Liu,¹ Hua Cheng,^{1,a)} Shuqi Chen,^{1,2,3,a)}  and Jianguo Tian^{1,2}

AFFILIATIONS

¹The Key Laboratory of Weak Light Nonlinear Photonics, Ministry of Education, School of Physics and TEDA, Institute of Applied Physics, Nankai University, Tianjin 300071, China

²Renewable Energy Conversion and Storage Center, Nankai University, Tianjin 300071, China

³The collaborative Innovation Center of Extreme Optics, Shanxi University, Taiyuan, Shanxi 030006, China

^{a)}Electronic addresses: hcheng@nankai.edu.cn and schen@nankai.edu.cn

ABSTRACT

Coding metasurfaces can combine simple logical bits to acquire sophisticated functions in wave control. Recently, coding metasurfaces have been demonstrated to take flexible control of the acoustic wave and realize intriguing functionalities such as wave branching, Fresnel lens, and asymmetric transmission. However, the previous design contains only two coding units, and thus, the resultant functions are relatively limited. Here, we propose the multi-bit coding acoustic metasurfaces to manipulate the reflection of acoustic waves. Theoretical predictions and experimental results are given to demonstrate the functions of wave branching and acoustic directionally propagating. We further perform digital convolution operations on the 3-bit coding metasurfaces and realize the generation and manipulation of an acoustic vortex beam. The presented design provides a flexible way for manipulating reflected acoustic waves and may find applications in construction engineering and particle trapping.

Published under license by AIP Publishing. <https://doi.org/10.1063/1.5087636>

Metasurfaces are kinds of planar metamaterials with a subwavelength thickness, which can provide space-dependent phase responses on the interface and manipulate the wavefront based on the phase shift accumulation along the surface. Compared to bulk metamaterials, metasurfaces are much smaller in volume and easier for fabrication, for which they can take deeper control of the wavefront and promote the development of small integrated devices. Driven by the original study of Yu *et al.*,¹ much effort has been paid to the research of metasurfaces for the manipulation of both electromagnetic and acoustic waves, which brought us numerous fascinating applications, including anomalous refraction and reflection,^{1–10} perfect absorption,^{10–13} holograms,^{14–17} and achromatic focusing.^{18–20}

Recently, digital and programmable metamaterials have been proposed for flexible control of the wavefront, termed as coding metamaterials.^{21–30} Different from traditional metasurfaces or metamaterials, the coding metamaterials allow the manipulation of waves in a real time way. The simplest 1-bit coding metamaterial contains two types of coding units “0” and “1,” which are defined according to the phase responses of 0 and π with correspondence to the states “on” and “off,” respectively. Since the initial proposal,²¹ coding metamaterials have developed rapidly in recent years in manipulating electromagnetic

waves and achieved many complicated functions, such as diffusion,²² steering,^{23–26} and vortex beam manipulation.^{27–30} Xie *et al.* first proposed the coding acoustic metasurfaces containing two types of coding elements with a π phase shift, which could realize compact functions on the transmitted wave, including wave branching, Fresnel lens, and asymmetric transmission.^{31,32} The concept was subsequently introduced to the topological insulators, which can flexibly control the acoustic propagation path through programming different coding sequences.³³ However, the previous coding acoustic metasurfaces are about the 1-bit coding with two kinds of coding units, which limit the realization of more complicated functions for practical use. Besides, the combination of the reflected acoustic waves and coding acoustic metasurfaces is also seldom studied, which is of great significance in applications such as echo chamber and indoor reverberation.

In this letter, we propose the multi-bit coding acoustic metasurfaces, which can contain eight or more types of coding units structured as Helmholtz resonators with different geometric parameters. Different from other metasurfaces for manipulating the acoustic reflection,^{6,7,10} we can take flexible control of the reflected acoustic waves by properly programming the coding sequences. The results are given in experiments, simulations, and theories, presenting good

accordance. Particularly, we further prove the generation and manipulation of the vortex beam by exquisite patterned coding metasurfaces, which provides a flexible way for particle trapping in the future.

We start with the design of structured coding units, which are fundamental building blocks for all the multi-bit coding acoustic metasurfaces. Specific structures characterized with the same reflection amplitude but different reflected phases are needed. For the N -bit coding metasurfaces, there are 2^N types of coding units, which have various phase responses with a gradient of $360^\circ/2^N$. Metasurfaces containing coding units are shown in Fig. 1(a), with the detailed coding unit structured as a Helmholtz resonator shown in Fig. 1(b), with a whole thickness of $h = 4.5$ mm ($\sim 0.1\lambda$) and a side length of $p = 25$ mm. The block neck has a changeable side length of d and a thickness of $t_1 = 1$ mm. The cylinder cavity has a radius of $r = 23$ mm and a height of $t_2 = 1$ mm. To analyze the reflection response of each coding unit, we use the COMSOL Multiphysics for the simulation, based on the finite-element method.³⁴ The material of the Helmholtz resonator is viewed as acoustically rigid,³¹ and the parameters of air used in the model are a sound speed of $c_0 = 343$ m/s, a mass density of $\rho = 1.21$ kg/m³, and a dynamic viscosity of $\mu = 1.56 \times 10^{-5}$ Pa s. By optimizing the geometric parameters, a phase variation range covering nearly 317° has been achieved at the frequency of 7000 Hz, illustrated in Fig. 1(c). As the loss in the reflection coefficient is only 6%, as shown in Fig. 1(d), we can leave out the thermal effects for the rest of the simulations. 2^N units with a $360^\circ/2^N$ phase gradient are obtained to work as the N -bit coding units. We take $N = 1, 2, 3$ for discussion. From Fig. 1(c), we can get the phase responses of $0^\circ, 45^\circ, 90^\circ, 135^\circ, 180^\circ, 215^\circ, 270^\circ,$ and 315° at side lengths $d = 0$ mm, 8.2 mm, 9.2 mm, 9.7 mm, 10.1 mm, 10.6 mm, 11.3 mm, and 14.7 mm, respectively. Thus, Helmholtz resonators with different d can be used as multi-bit coding units, which are clearly illustrated in Table I. The proposed Helmholtz resonators can also be used as higher-bit coding units.

Now, we can program metasurfaces with designed coding units. For 1-bit coding metasurfaces, we use a 2×2 sub-array of bits “0” or “1” as a lattice; then, $M \times M$ equal-sized lattices can be arbitrarily

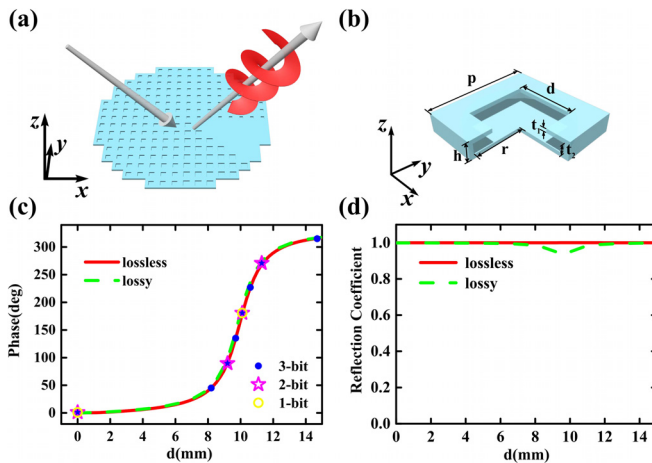


FIG. 1. The schematic of the planar (a) coding metasurfaces and (b) coding unit. Simulated (c) reflected phases and (d) reflection coefficients versus neck side lengths of a Helmholtz resonator at 7000 Hz, in both the lossless and lossy model.

TABLE I. Designed 1-, 2-, and 3-bit coding units using Helmholtz resonators with different scales.

Multi-bit	d (mm)							
	0	8.2	9.2	9.7	10.1	10.6	11.3	14.7
1-bit	0				1			
2-bit	00		01		10		11	
3-bit	000	001	010	011	100	101	110	111

distributed to make different coding sequences. The reflected phase of the mn lattice $\varphi(m, n)$ is either 0° or 180° . The far-field scattering pattern can be expressed as³¹

$$f(\theta, \varphi) = f_e(\theta, \varphi) \sum_{m=1}^N \sum_{n=1}^N \exp \left\{ -i\varphi(m, n) - ikP \sin \theta \left[\left(m - \frac{1}{2} \right) \cos \varphi + \left(n - \frac{1}{2} \right) \sin \varphi \right] \right\}, \quad (1)$$

where θ and φ are the elevation and azimuth angle of an arbitrary direction, respectively, P is the lattice side length equal to $2p$, and $f_e(\theta, \varphi)$ is the pattern function of a lattice. Here, three sequences of 0000.../0000..., 0101.../0101... and 0101.../1010... are discussed. For 2-bit coding metasurfaces, a unit works as a lattice. The sequence of 11 10 01 00.../11 10 01 00... in the x -direction is selected for discussion. By applying Fermat’s principle, generalized Snell’s law predicts the reflection angle to be⁶

$$\theta_r = \arcsin \left(\frac{1}{k} \frac{d\phi(x)}{dx} \right), \quad (2)$$

where k is the acoustic wave vector in air and $d\phi(x)$ and dx represent the phase shift and the distance between two cross points along the x direction, respectively.

To experimentally understand the functions of the coding metasurfaces, we use a plane wave to illuminate normally on the interface. As Fig. 2(a) shows, a circular planar speaker (JBL CSS8006BM, diameter 200 mm) is used as the sound source. The measurement of the acoustic field is accomplished by two microphones (B&K 4961, 1/4-in. diameter), one of which is fixed to serve as the phase reference and the other one scans the field point by point. A multianalyzer system (B&K Type 3560B) is used to analyze the measuring sound signal, with which the amplitude and phase of the wave are separately extracted. Photographs of coding metasurface samples are shown in Fig. 2(b), which are fabricated with polylactic acid (PLA), utilizing the three-dimensional (3D) printing technique (Ultimaker 2+, with 0.02 mm precision).

Figure 3 shows the simulated and experimental far-field scattering patterns [Figs. 3(a)–3(h)] and near-field pressure distributions [Figs. 3(i)–3(o)]. For 1-bit coding metasurfaces, we can deduce the far-field patterns from Eq. (1) with different arrays of $\varphi(m, n)$. For example, when the sequence is 0000.../0000..., the reflected phase $\varphi(m, n)$ equals 0° for each lattice, and thus, the scattering pattern can be obtained as

$$|f_1(\theta, \varphi)| = C_1 |\cos \psi_1 + \cos \psi_2|, \quad (3)$$

where $\psi_1 = kP(\sin \theta \cos \varphi + \sin \theta \sin \varphi)/2$ and $\psi_2 = kP(-\sin \theta \cos \varphi + \sin \theta \sin \varphi)/2$, respectively. Obviously, the function can reach its

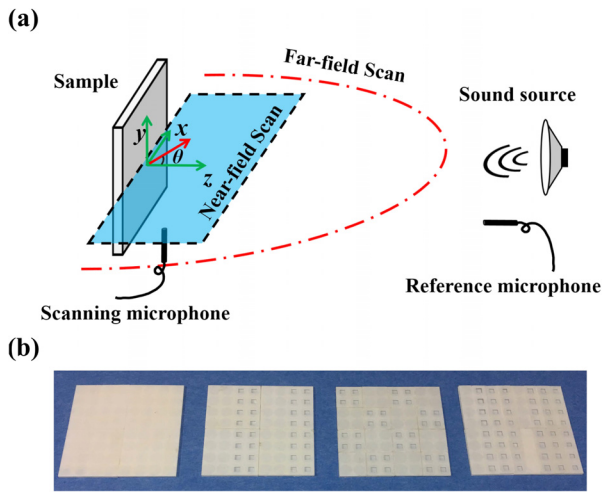


FIG. 2. (a) Schematic of the experimental setup. (b) Photograph of four samples of designed metasurfaces with coding sequences 0000.../0000..., 0101.../0101..., 0101.../1010..., 00 01 10 11.../00 01 10 11...; all samples have a side length of 200 mm.

maximum when $\theta=0^\circ$. Therefore, the acoustic wave is mainly reflected back along the incident direction, which can also be confirmed by the 3D and two-dimensional (2D) far-field patterns shown in Figs. 3(a) and 3(e). Figures 3(i) and 3(m) further present the

acoustic pressure distributions of reflected acoustic waves in the x - z cutting plane. Similarly, the far-field patterns for metasurfaces with sequences of 0101.../0101... and 0101.../1010... can also be derived, respectively, as $|f_2(\theta, \varphi)| = C_2 |\sin \psi_1 + \sin \psi_2|$ and $|f_3(\theta, \varphi)| = C_3 |\cos \psi_1 - \cos \psi_2|$. We get the maximums at $\theta_2 = 29.3^\circ$, $\varphi_2 = 90^\circ$, and 270° for 0101.../0101..., $\theta_3 = \arcsin(\lambda/\Gamma) = \arcsin(\lambda/2P) = 43.9^\circ$, $\varphi_3 = 45^\circ, 135^\circ, 225^\circ$, and 315° for 0101.../1010..., respectively. Thus, the normally incident wave is mainly reflected into two (four) symmetrically oriented directions, as illustrated in Figs. 3(b) and 3(f) [Figs. 3(c) and 3(g)]. Figures 3(j) and 3(n) [Figs. 3(k) and 3(o)] show the corresponding near-field pressure distributions of reflected acoustic waves in the x - z ($y=x$) cutting plane. The normally incident plane wave deflects to two quasi-plane waves propagating to two symmetric directions, forming a standing-wave like in the central area. It is worth noting that the metasurface with a sequence of 0000.../0000... works as a reflector, which is easy to understand as the structure is just a plate. The branching effect of metasurfaces with the sequence 0101.../0101... and 0101.../1010... can be explained as the interference of coding units “0” and “1,” which characterized by an opposite phase response of 0° and 180° . For 2-bit coding metasurface with a sequence 11 10 01 00.../11 10 01 00... in the x -direction, the reflected angle can be calculated by Eq. (2) as $\theta_4 = -29.3^\circ$, which agrees well with the simulated and experimental results shown in Figs. 3(d) and 3(h). Figures 3(l) and 3(p) show the corresponding acoustic pressure distributions of the reflected wave, from which the reflected wave is observed as a plane wave oblique to the surface normal under the normal incidence. This anomalous reflection effect results from

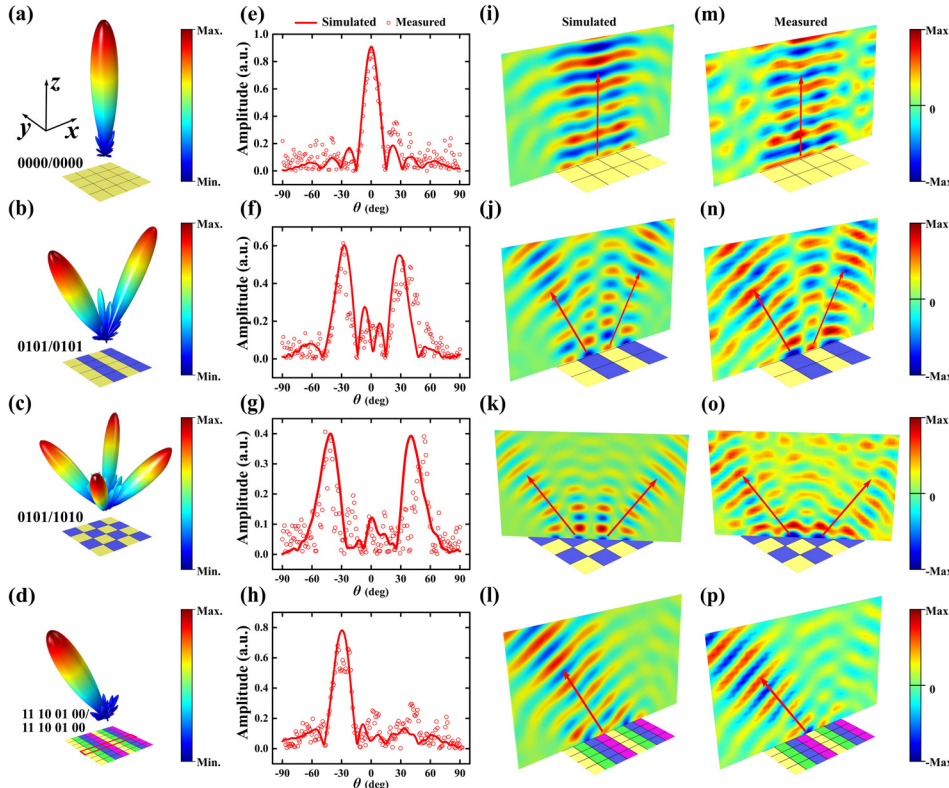


FIG. 3. (a)–(d) Simulated 3D far-field scattering patterns of a coding metasurface with a sequence of (a) 0000.../0000..., (b) 0101.../0101..., (c) 0101.../1010..., and (d) 00 01 10 11.../00 01 10 11... (e)–(h) The corresponding simulated and measured 2D far-field patterns. (i)–(l) Simulated and (m)–(p) measured near-field pressure distributions of a coding metasurface with a sequence of (i) and (m) 0000.../0000..., (j) and (n) 0101.../0101..., (k) and (o) 0101.../1010..., and (l) and (p) 00 01 10 11.../00 01 10 11...

the phase gradient on the interface and allows the metasurface to serve as a directional acoustic wave transmitter. Additionally, we calculated the efficiencies of wave splitting for coding sequences 0000.../0000..., 0101.../0101..., 0101.../1010... as 99%, 97%, 97%, respectively; the efficiency of anomalous reflection for coding sequence 11 10 01 00.../ 11 10 01 00... is 94%. It is easy to understand that the efficiencies are very high because the reflection coefficient of each coding unit is close to 1.

When 3-bit coding metasurfaces are utilized, eight types of coding units are contained and the obtained discrete phase units are more continuous than 1-bit and 2-bit situations. Thus, more complicated patterns and functions can be achieved with the 3-bit coding units. Recently, researches on generating the acoustic vortex beams have received attentions because acoustic vortex beams are very useful in particle trapping.^{35,36} By utilizing the 3-bit coding units, a simple and passive way to manipulate the vortex beam can be achieved. Like the vortex beam in optics,^{1,25} the acoustic vortex beam also has an azimuthal phase dependence $\exp(il\varphi)$ and carrying an orbital angular momentum (OAM). A direct method to create the acoustic vortex beam is introducing a spiral-like phase shift through a metasurface, in which the phase distribution is expressed as $\Phi(x, y) = l\varphi = l \cdot \arctan(y/x)$, where l is the topological charge.²⁵ The OAM metasurface pattern is shown in Fig. 4(a), where “0” to “7” represent “000” to “111,” respectively. Obviously, the

interface introduces a spiral-like phase shift with respect to the planar wavefront of the normally incident acoustic wave, thus creating a vortex beam with $l = 1$, with the simulated 3D scattering pattern shown in Fig. 4(b). The vortex beam has an annular intensity distribution in the cross-section, which can be seen from the near-field intensity distribution in the simulated [Fig. 4(c)] and theoretical [Fig. 4(e)] results, respectively. The spiral wavefront of the vortex beam can also be confirmed from the simulated [Fig. 4(d)] and theoretical [Fig. 4(f)] results.

More interestingly, by making convolution operations on 3-bit coding metasurfaces, the manipulation of an acoustic vortex beam can be achieved. As we know, the convolution in the frequency domain is equivalent to the ordinary multiplication in the corresponding time domain. When the single-frequency plane wave operates, we have

$$f(t) \cdot e^{i\omega_0 t} \xleftrightarrow{FFT} f(\omega) * \delta(\omega - \omega_0) = f(\omega - \omega_0). \quad (4)$$

Since there exists a Fourier transform relation between the far-field pattern and the coding pattern, convolution operations can also be used in the coding metasurfaces. As illustrated in Fig. 5, we add a gradient phase pattern “6 4 2 0.../6 4 2 0...” along the x -direction [Fig. 5(a)] to the OAM metasurface [Fig. 5(b)], obtaining a metasurface with a mixed coding pattern shown in Fig. 5(c). The coding pattern in Fig. 5(a) could reflect the normally incident plane wave to an

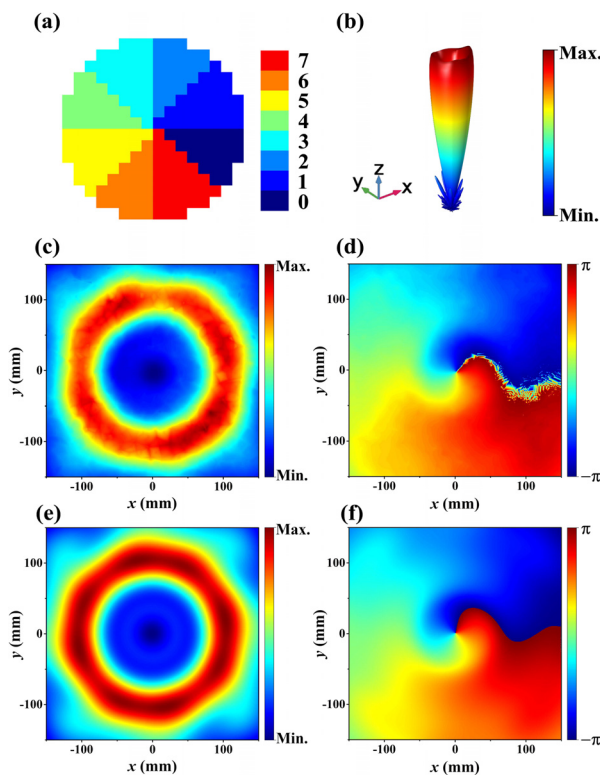


FIG. 4. The generation of an acoustic vortex beam by a 3-bit coding metasurface. (a) Coding pattern with $l = 1$. (b) Simulated 3D scattering pattern and the vortex acoustic beam propagating towards the positive z -axis. (c) and (d) Simulated and (e) and (f) theoretical near-field intensity and phase distributions in the x - y plane with $z = 43$ cm.

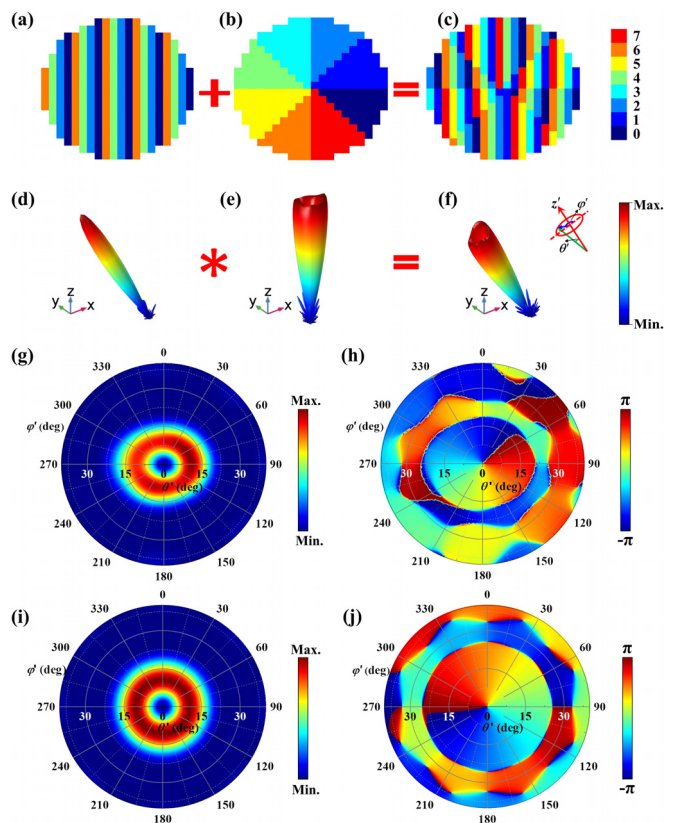


FIG. 5. Control of the orientation of the acoustic vortex beam. (a)–(c) The coding patterns. (d)–(f) Simulated 3D scattering results. (g) and (h) Simulated and (i) and (j) theoretical far-field intensity and phase distributions.

anomalous direction with an angle of -29.3° to the z -axis, as the 3D far-field scattering pattern shown in Fig. 5(d). Thus, with convolution operations, the mixed metasurface can create a vortex beam with a reflected angle of -29.3° to the z -axis, which can be seen from the simulated 3D far-field scattering pattern shown in Fig. 5(f). Figures 5(g)–5(j) further illustrate the simulated and theoretical far-field distributions of intensity and phase, where θ' and φ' are the elevation and azimuthal angles with respect to the propagating z' axis, respectively. The central region of the beam is clearly observed to be “dark” with a zero intensity from both simulation [Fig. 5(g)] and theory [Fig. 5(i)], which is consistent with the characteristics of vortex beams. In addition, the simulated [Fig. 5(h)] and theoretical [Fig. 5(j)] far-field phase distributions are observed to be spiral-like, which change from 0° to 360° when the azimuthal angle φ' varies from 0 to 2π . It can be deduced that we can control the propagating direction of the vortex beam by adding different coding patterns to the OAM metasurface, and even we can create multi-vortex beams.

In conclusion, we proposed the multi-bit acoustic coding metasurfaces based on Helmholtz resonators. Our design is demonstrated to be able to generate arbitrary shapes of the reflected wavefront. As examples, we theoretically and experimentally prove the functions of wave branching and directionally propagating. Moreover, we give a theoretical demonstration of the generation and manipulation of the acoustic vortex beam with the aid of 3-bit coding units and the digital convolution operations on the coding metasurfaces. Last but not least, the thermoviscous effects are considered and demonstrated to have little impact, promising strong practicality. The proposed multi-bit acoustic coding metasurfaces provide a flexible way for the manipulation of reflected acoustic waves with high efficiency, which may promote the development of acoustic chips carrying compact functions with wide prospect for applications in wave field modulations, construction engineering, and particle trapping.

This work was supported by the National Key Research and Development Program of China (Nos. 2016YFA0301102 and 2017YFA0303800), the National Natural Science Foundation of China (Nos. 91856101, 11774186, and 11574163), the Natural Science Foundation of Tianjin for Distinguished Young Scientists (No. 18JJCQJC45700), the Natural Science Foundation of Tianjin (No. 16JJCQNJC01700), and the 111 Project (No. B07013).

REFERENCES

- N. Yu, P. Genevet, M. A. Kats, F. Aieta, J. P. Tetienne, F. Capasso, and Z. Gaburro, *Science* **334**, 333 (2011).
- L. Huang, X. Chen, H. Mühlenbernd, G. Li, B. Bai, Q. Tan, G. Jin, T. Zentgraf, and S. Zhang, *Nano Lett.* **12**, 5750 (2012).
- X. Ni, N. K. Emani, A. V. Kildishev, A. Boltasseva, and V. M. Shalaev, *Science* **335**, 427 (2012).
- N. Meinzer, W. L. Barnes, and I. R. Hooper, *Nat. Photonics* **8**, 889 (2014).
- Z. Li, H. Cheng, Z. Liu, S. Chen, and J. Tian, *Adv. Opt. Mater.* **4**, 1230 (2016).
- Y. Li, B. Liang, Z. M. Gu, X. Zou, and J. Cheng, *Sci. Rep.* **3**, 2546 (2013).
- J. Zhao, B. Li, Z. Chen, and C. W. Qiu, *Sci. Rep.* **3**, 2537 (2013).
- K. Tang, C. Qiu, M. Ke, J. Lu, Y. Ye, and Z. Liu, *Sci. Rep.* **4**, 6517 (2014).
- Y. Li, C. Shen, Y. Xie, J. Li, W. Wang, S. A. Cummer, and Y. Jing, *Phys. Rev. Lett.* **119**, 35501 (2017).
- Y. Zhu, X. Fan, B. Liang, J. Cheng, and Y. Jing, *Phys. Rev. X* **7**, 021034 (2017).
- Y. Yao, R. Shankar, M. A. Kats, Y. Song, J. Kong, M. Loncar, and F. Capasso, *Nano Lett.* **14**, 6526 (2014).
- J. Li, P. Yu, C. Tang, H. Cheng, J. Li, S. Chen, and J. Tian, *Adv. Opt. Mater.* **5**, 1700152 (2017).
- Y. Tang, S. Ren, M. Han, F. Xin, L. Huang, T. Chen, C. Zhang, and T. J. Lu, *Sci. Rep.* **7**, 43340 (2017).
- G. Zheng, H. Mühlenbernd, M. Kenney, and G. Li, *Nat. Nanotechnol.* **10**, 308 (2015).
- X. Ni, A. V. Kildishev, and V. M. Shalaev, *Nat. Commun.* **4**, 2807 (2013).
- Y. Zhu, J. Hu, X. Fan, J. Yang, B. Liang, X. Zhu, and J. Cheng, *Nat. Commun.* **9**, 1632 (2018).
- Y. Xie, C. Shen, W. Wang, J. Li, D. Suo, B. I. Popa, Y. Jing, and S. A. Cummer, *Sci. Rep.* **6**, 35437 (2016).
- W. T. Chen, A. Y. Zhu, V. Sanjeev, M. Khorasaninejad, Z. Shi, E. Lee, and F. Capasso, *Nat. Nanotechnol.* **13**, 220 (2018).
- S. Wang, P. C. Wu, V. C. Su, Y. C. Lai, M. K. Chen, H. Y. Kuo, B. H. Chen, Y. H. Chen, T. T. Huang, J. H. Wang, R. M. Lin, C. H. Kuan, T. Li, Z. Wang, S. Zhu, and D. P. Tsai, *Nat. Nanotechnol.* **13**, 227 (2018).
- Y. F. Zhu, X. Y. Zou, R. Q. Li, X. Jiang, J. Tu, B. Liang, and J. Cheng, *Sci. Rep.* **5**, 10966 (2015).
- T. J. Cui, M. Q. Qi, X. Wan, J. Zhao, and Q. Cheng, *Light Sci. Appl.* **3**, e218 (2014).
- L. H. Gao, Q. Cheng, J. Yang, S. J. Ma, J. Zhao, S. Liu, H. B. Chen, Q. He, W. X. Jiang, H. F. Ma, Q. Y. Wen, L. J. Liang, B. B. Jin, W. W. Liu, L. Zhou, J. Q. Yao, P. H. Wu, and T. J. Cui, *Light Sci. Appl.* **4**, e324 (2015).
- S. Liu, T. J. Cui, Q. Xu, D. Bao, L. Du, X. Wan, W. X. Tang, C. Ouyang, X. Y. Zhou, H. Yuan, H. F. Ma, W. X. Jiang, J. Han, W. Zhang, and Q. Cheng, *Light Sci. Appl.* **5**, e16076 (2016).
- S. Liu, L. Zhang, Q. L. Yang, Q. Xu, Y. Yang, A. Noor, Q. Zhang, S. Iqbal, X. Wan, Z. Tian, W. X. Tang, Q. Cheng, J. G. Han, W. L. Zhang, and T. J. Cui, *Adv. Opt. Mater.* **4**, 1965 (2016).
- S. Liu, H. C. Zhang, L. Zhang, Q. L. Yang, Q. Xu, J. Gu, Y. Yang, X. Y. Zhou, J. Han, Q. Cheng, W. Zhang, and T. J. Cui, *ACS Appl. Mater. Interfaces* **9**, 21503 (2017).
- S. Liu, T. J. Cui, L. Zhang, Q. Xu, Q. Wang, X. Wan, J. Q. Gu, W. X. Tang, M. Q. Qi, J. G. Han, W. L. Zhang, X. Y. Zhou, and Q. Cheng, *Adv. Sci.* **3**, 1600156 (2016).
- L. Zhang, S. Liu, L. Li, and T. J. Cui, *ACS Appl. Mater. Interfaces* **9**, 36447 (2017).
- L. Zhang, R. Y. Wu, G. D. Bai, H. T. Wu, Q. Ma, X. Q. Chen, and T. J. Cui, *Adv. Funct. Mater.* **28**, 1802205 (2018).
- Q. Ma, C. B. Shi, G. D. Bai, T. Y. Chen, A. Noor, and T. J. Cui, *Adv. Opt. Mater.* **5**, 1700548 (2017).
- L. Zhang, X. Q. Chen, S. Liu, Q. Zhang, J. Zhao, J. Y. Dai, G. D. Bai, X. Wan, Q. Cheng, G. Castaldi, V. Galdi, and T. J. Cui, *Nat. Commun.* **9**, 4334 (2018).
- B. Xie, K. Tang, H. Cheng, Z. Liu, S. Chen, and J. Tian, *Adv. Mater.* **29**, 1603507 (2017).
- B. Xie, H. Cheng, K. Tang, Z. Liu, S. Chen, and J. Tian, *Phys. Rev. Appl.* **7**, 024010 (2017).
- J. P. Xia, D. Jia, H. X. Sun, S. Q. Yuan, Y. Ge, Q. R. Si, and X. J. Liu, *Adv. Mater.* **30**, 1805002 (2018).
- COMSOL, Inc., *COMSOL Multiphysics, Version 5.2a* (COMSOL, Inc., Burlington, MA, 2016).
- A. Marzo, M. Caleap, and B. W. Drinkwater, *Phys. Rev. Lett.* **120**, 44301 (2018).
- C. Shi, M. Dubois, Y. Wang, and X. Zhang, *Proc. Natl. Acad. Sci.* **114**, 7250–7253 (2017).